Journal of Catalysis **209,** 385–393 (2002)
doi:10.1006/jcat.2002.3639

The Location and Effects of Coke Deposition in Fluid Cracking Catalysts during Gas Oil Cracking at Microactivity Test Conditions

M. L. Occelli,*,[1] J. P. Olivier,† and A. Auroux‡

*MLO Consulting, 6105 Black Water Trail, Atlanta, Georgia 30328; †Micromeritics Instrument Corporation Inc., Norcross, Georgia 30093; and ‡Institut de Recherches sur la Catalyse, CNRS, 2 Avenue A. Einstein, 69626 Villeurbanne, France

Received November 12, 2001; revised April 2, 2002; accepted April 11, 2002

Nitrogen porosimetry, atomic force microscopy (AFM), and microcalorimetry together with microactivity testing have been used to characterize some of the effects of coke deposition on a fluid cracking catalyst (FCC) during gas oil cracking. Contact mode AFM images have revealed that coke forms raised surface features consisting of molecules and chain of molecules; evidence of pore blockage by coke deposits could not be obtained in the images generated. Nitrogen porosimetry results indicate that during gas oil cracking, coke is deposited inside (68%) as well as outside (32%) the catalyst porous structure. About 60% of the total coke in the porous structure is uniformly deposited within its microspace, decreasing the micropore volume and causing a shift of its pore size distribution profile toward smaller pore width values. The rest of the coke (40%) is located in mesopores without closing any part of the internal porosity to nitrogen sorption and therefore to catalysis. There is a moderate decrease in acid site strength and acid site density in the coked FCC. Both BET and Langmuir methods grossly underestimate the FCC surface area and only the density functional theory method yields reliable surface area and pore volume measurements over the entire micro–meso porosity range.

INTRODUCTION

Easy accessibility of active sites in the internal porosity of fluid cracking catalysts (FCCs) is essential to the efficient and selective cracking of gas oils to gasoline and other valuable products (1). Coke formation on heterogeneous catalysts has traditionally been investigated by infrared and X-ray photoelectron spectroscopies. Imaging of coked surfaces has been accomplished using scanning tunneling microscopy (2) and high-resolution electron microscopy (3). Micrometer-scale ($5 \times 5\ \mu$m) atomic force microscopy (AFM) images have shown that on a partial oxidation catalyst such as MoO_3, coke deposition forms 10-nm particles organized in rows parallel to the [010] direction of the crystal (4). In contrast, coke deposition, from gas oil cracking at microactivity testing (MAT) conditions, over pillared clays generates a spent catalyst coated with a surface layer of coke; the nature of the coke layer is not known. In the case of a pillared rectorite catalyst, nanometer-scale AFM images have indicated a preferential deposition of carbonaceous residues near the three basal oxygens of SiO_4 units that form the clay silicate layers (5). The images obtained exhibit a geometry similar to graphite and consist of white spots arranged in a distorted but easily recognizable hexagonal arrangement. Repeat distances in the image are larger then those measured for the steam-aged clay catalyst before MAT evaluation and much larger than those in graphite (5).

During gas oil cracking the continuous deposition of coke may prevent the diffusion and cracking of high molecular weight hydrocarbons to the catalyst internal porosity owing to pore plugging or fouling (1). Recently, contrast-matching small-angle neutron scattering (CM-SANS) techniques have been used to investigate the relationship between coking and porosity losses in FCCs (6). SANS has indicated that the level of closed porosity in a partially stripped deactivated FCC is high and that the amount of closed porosity decreased with increased stripping severity (6).

The conventional approach to study porosity losses in heterogeneous catalysts is to monitor the reduction of surface area and pore volume by nitrogen porosimetry (1) experiments. For nonmicroporous solids the BJH method (7) is frequently used to obtain surface area (*SA*) and total pore volume (*PV*) distribution data from experimental sorption isotherms. Other frequently used methods such as the Langmuir (8) and BET (9) formalisms are based on the model of adsorption on a free surface. The Langmuir model assumes the surface saturates after the first adsorbed layer, while the BET model presumes that multilayers can form at higher pressures. However, neither model allows for the filling of micropores. Thus surface areas derived from these two models will differ from the actual area in a way that depends on the solid microporous structure.

It is the purpose of this paper to report the loss of acidity and porosity in a commercial FCC sample owing to coke formation and deposition during gas oil cracking at MAT conditions. Surface area and pore volume distribution over

[1] To whom correspondence should be addressed.

0021-9517/02 $35.00

the entire micro–meso porosity range will be investigated with a nonlocal density functional theory (DFT) model (10) while acidity will be determined from microcalorimetry experiments using ammonia as the probe molecule (11, 12).

EXPERIMENTAL

Microactivity Testing

The commercial FCC under study contains, as its cracking component, 20–30 wt% of an HY-type zeolite stabilized by low levels of rare earth (RE) cations, together with >50 wt% kaolin. The rest is an aluminosilicate gel that keeps the FCC components together; some properties of this FCC are given in Table 1. The fresh FCC was steam aged for 5 h at 760°C with 100% steam at 1 atm. Microactivity testing of the steam-aged FCC was conducted with a Kuwait vacuum gas oil (VGO) using a reactor temperature of 537°C, 60-s injection time, and a cat/oil (C/O) ratio of ~3.0. After gas oil cracking, the spent catalyst (~3.6 g) was stripped for 15 min with a flow of 100 cm^3 nitrogen/min at 537°C to remove occluded hydrocarbons.

Nitrogen Porosimetry

Nitrogen sorption isotherms obtained at liquid nitrogen temperature were collected using a volumetric technique on a Micromeritics ASAP 2010 adsorption instrument equipped with the micropore options. Prior to analysis, samples weighing from 0.1 to 0.3 g were outgassed in vacuum at 300°C for at least 16 h. PV was derived from the amount of nitrogen adsorbed at a relative pressure close to unity ($p/P_o = 0.995$) by assuming that all the accessible pores were then filled with liquid nitrogen. SA measurements were performed using the BET and Langmuir equations and were compared with results obtained with DFT methods (13). The BJH method was not considered applicable since the catalyst under study is essentially a microporous solid; PV and SA data are presented in Tables 2 and 3.

TABLE 1

Some Properties of the Fresh Commercial FCC under Study

Total SA = 227 m^2/g
Zeolite SA = 173 m^2/g
Matrix SA = 54 m^2/g
Crystallinity (XRD) = 31.5%
Pore volume = 0.370 ml/g
ABD = 0.82 g/cm^3
APS (PSD) = 7.26 nm
RE_2O_3 = 2.32 wt%
Al_2O_3 = 34.01 wt%
Na_2O = 0.34 wt%
Fe_2O_3 = 0.51 wt%
Attrition Index (AI) = 2.8

TABLE 2

Surface Area (SA, m^2/g) and Pore Volume (PV, cm^3/g) Results from Nitrogen Porosimetry Data for the Steam-Aged FCC before MAT Evaluation

Method	Micro. SA	Total SA	Micro. PV	Total PV[a]
DFT	385	396	0.075	0.118
Langmuir	—	203	—	—
BET	—	172	—	—
t-plot	143	172	0.060	—
D–R	213	—	0.075	—

[a] Measured at $p/P_o = 0.995$.

Microcalorimetry

Heats of NH_3 adsorption were measured using a heat-flow microcalorimeter from Setaram, linked to a glass volumetric line. Successive doses of gas were admitted to the sample until a final equilibrium pressure of 133 Pa was obtained. The equilibrium pressure relative to each adsorbed amount was measured by means of a differential pressure gauge from Datametrics. The adsorption temperature was maintained at 200°C. Primary and secondary isotherms were collected at this temperature. Similarly to the pretreatment used to prepare the samples for nitrogen porosimetry, all samples were degassed overnight under vacuum at 300°C before calorimetric measurements were undertaken. Microcalorimetry results are in Table 4.

Atomic Force Microscopy

The AFM used in this work was a Nanoscope III instrument (from Digital Instruments, Santa Barbara, CA) operating in contact mode; the AFM was calibrated using mica. The images presented in this paper contain either 256 × 256 or 512 × 512 data points and were obtained within a few seconds. The Si_3N_4 cantilever (with integral tip) had a length in the 60–120 μm range with spring constants in the

TABLE 3

Surface Area (SA, m^2/g) and Pore Volume (PV, cm^3/g) Results from Nitrogen Porosimetry Data for the Steam-Aged FCC after MAT Evaluation and Coking

Method	Micro. SA	Total SA	Micro. PV	Total PV[a]
DFT	371	381	0.066	0.103
Langmuir	—	171	—	—
BET	—	144	—	—
t-plot	120	144	0.051	—
D–R	175	—	0.062	—

[a] Measured at $p/P_o = 0.995$.

TABLE 4

Ammonia Chemisorption Data at 200°C ($p = 27$ Pa)

					kJ/mol		
	H_{in}	H_{int}	V_T	V_{Irr}	<100	100–150	>150
Steam-aged FCC	156	7.4	132	55	113	11	8
Coked FCC	144	6.4	124	55	110	14	0

Note. Initial heats (H_{in}) are in kJ/mol. Integral heats (H_{int}) are in J/g. V_T, V_{Irr}, and the population of sites with a given strength are in μmol NH_3/g.

0.1–0.6 N/m range. Typical forces applied to obtain these images ranged from 1.0 to 100 nN. In order to avoid tip-related artifacts, imaging was performed with minimal (less then 10 nN) force and image features were reproduced before being accepted as representative. Moreover, by rotating the image, changing scan speeds and time, changing imaging forces and, acquiring images invariant with time, it is believed that artifacts can be identified and separated from real features when studying the surfaces of FCCs with an AFM operating in contact mode.

RESULTS AND DISCUSSION

The commercial FCC under study initially has an ivory coloration and cracks a Kuwait gas oil at MAT conditions with 75.1 wt% conversion. Gasoline, light cycle gas oil (LCGO), and slurry oil (SO) generation was 48.5, 13.3, and 11.6 wt% respectively. The used FCC contains 3.5 wt% coke, which imparts a dark black coloration to the catalyst. When the steam-aged and coked FCC samples are heated to ~300°C in the presence of ~30% He/70% O_2, the two samples generate TG and DTG profiles (not shown) that almost overlap; then in the 350–630°C temperature range, the coked FCC undergoes a ~3.4% weight loss, in good agreement with the 3.5% coke content. In the same temperature range, the DTG profile shows the existence of a broad asymmetric exotherm with a peak maximum near 540°C attributed to the oxidative decomposition of carbonaceous deposits in the catalysts porous structure.

Atomic Force Microscopy

Large-scale, contact mode AFM images of the steam-aged FCC under study contain topographical details

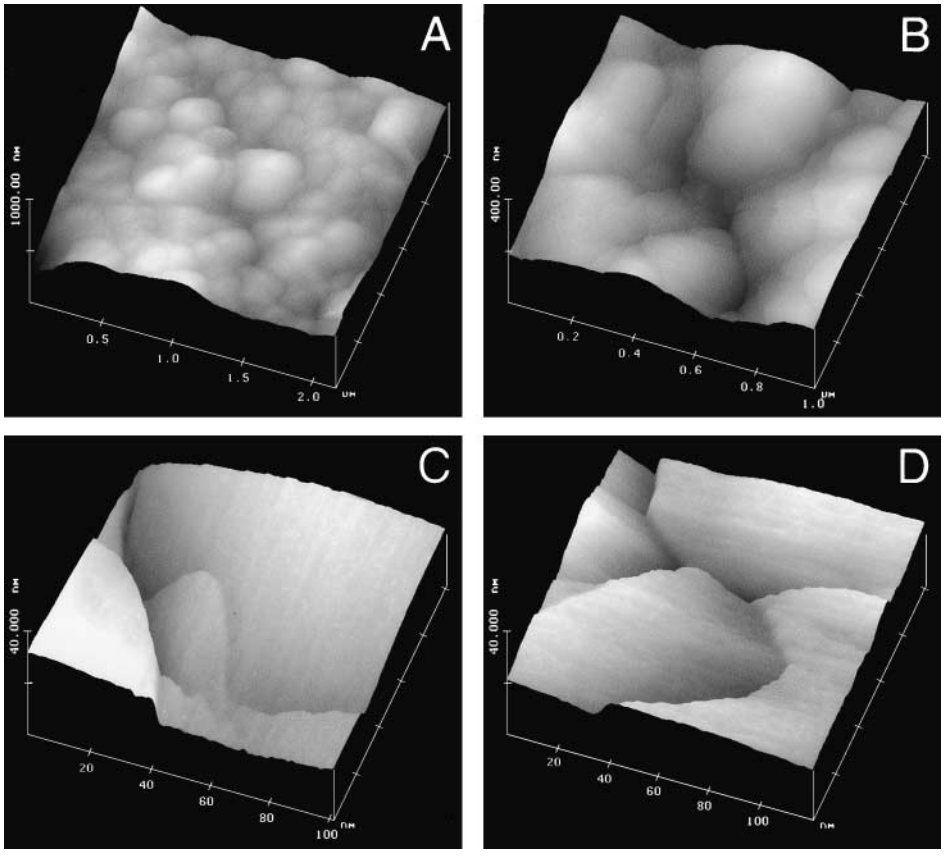

FIG. 1. Contact mode, micrometer-scale AFM image of the steam-aged FCC showing (A) the aggregation of particles on the FCC surface and (B) surface defects. The contact mode, nanometer-scale AFM images in (C) and (D) give a typical representation of the surface porosity in steam-aged FCCs.

already observed in other type of FCCs (14–16). In fact, the surface of the steamed FCC appears to be fairly heterogeneous and composed of an agglomeration of particles; these particles consist of stacks of clay platelets (14). In Fig. 1A the mean surface area of the particles is 250 nm^2. Missing particles (or platelets) can generate surface craters or deep valleys that can be 450 nm wide and 110 nm deep (Fig. 1B). At a greater magnification (100 × 100 nm) it can be observed that voids between particles (or platelets) generate cracks 15–20 nm wide and these are responsible for the surface porosity of the catalyst (Fig. 1C). The porosity of the surface is further illustrated in Fig. 1D. In all cases, pores on the FCC surface are long cracks with width w and length D such that $w/D \ll 1$. Similar images have been obtained for other types of commercially available FCCs (14–16).

Coke deposition on the FCC surface results in a decrease in surface roughness owing to a fairly homogeneous distribution of coke deposits; however, the coked surface retains the main topographical features seen in the steam-aged FCC (Figs. 1A–1D). That is, it is still possible to observe that missing plates (or particles) from the surface can form large craters about 1 μm wide and 150 nm deep (Fig. 2A). The stacking of plates (probably Kaolin, a major component of the catalyst) and elongated surface cracks (pores) are still evident in Fig. 2B. The nanometer-scale image in Fig. 2C provides a representative description of the surface porosity in the coked FCC. In addition to cracks <10 nm wide with $w/D \ll 1$, it is sometime possible to observe pores 10–15 nm in diameter, as shown in Fig. 2D. In the nanometer-scale image shown in Fig. 3 the coked surface is represented by raised surface features that resemble fibrils formed by chains of molecules and chain aggregates that prevent the observation of the molecular-scale parameters of the clay surface (5). Evidence of pore blockage on the FCC surface owing to coke deposits could not be observed in any image generated.

Although AFM can reveal the surface topography of a catalyst with unprecedented resolution it cannot provide any information concerning its chemical composition. Similarly, with only 3.5 wt% coke even NMR cannot generate detailed structural information of the coke present. In fact, after 5 days of data acquisition the S/N ratio in the ^{13}C-CP-MAS spectrum of the coked FCC (not shown) was found to be very poor (17); only its signal at 122 ppm can be safely assigned to the presence of aliphatic chains. The ^{1}H-NMR spectrum of the coked FCC (not shown) contains a line

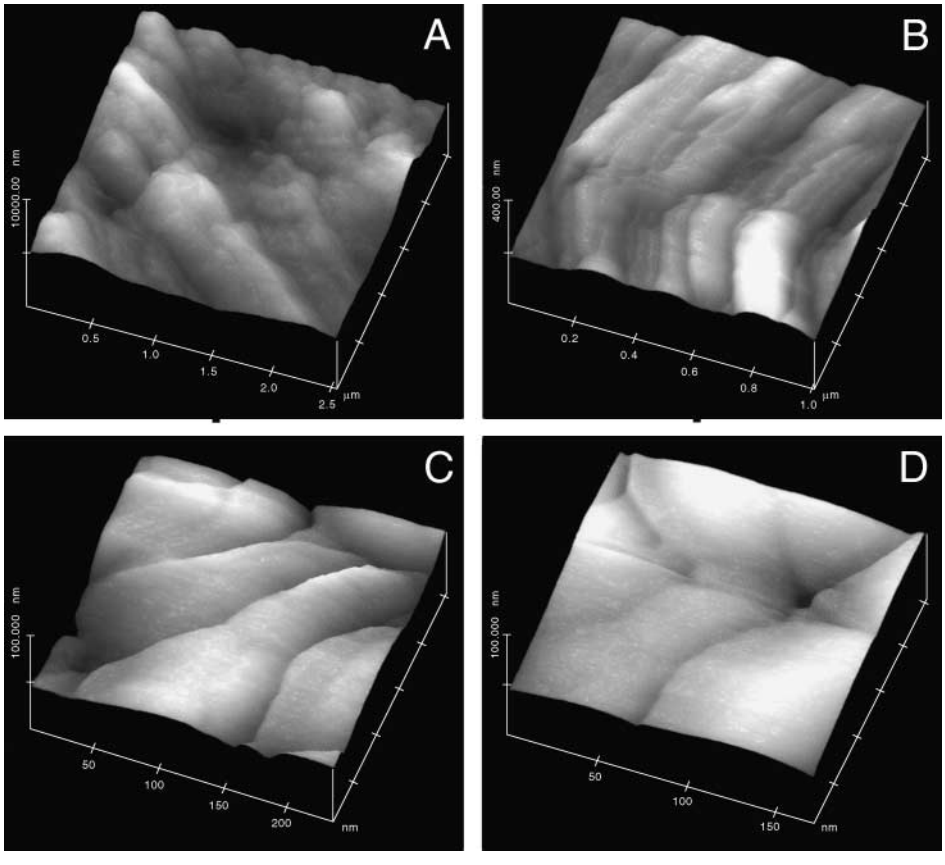

FIG. 2. Contact mode, micrometer-scale AFM image of the FCC surface after steaming, MAT evaluation, and coke deposition. The spent catalyst contains 3.5 wt% coke. (A) Surface defects of the coked FCC surface; (B) plates (probably Kaolin) agglomeration. The contact mode, nanometer-scale AFM images in (C) and (D) give a typical representation of the surface porosity in coked FCCs.

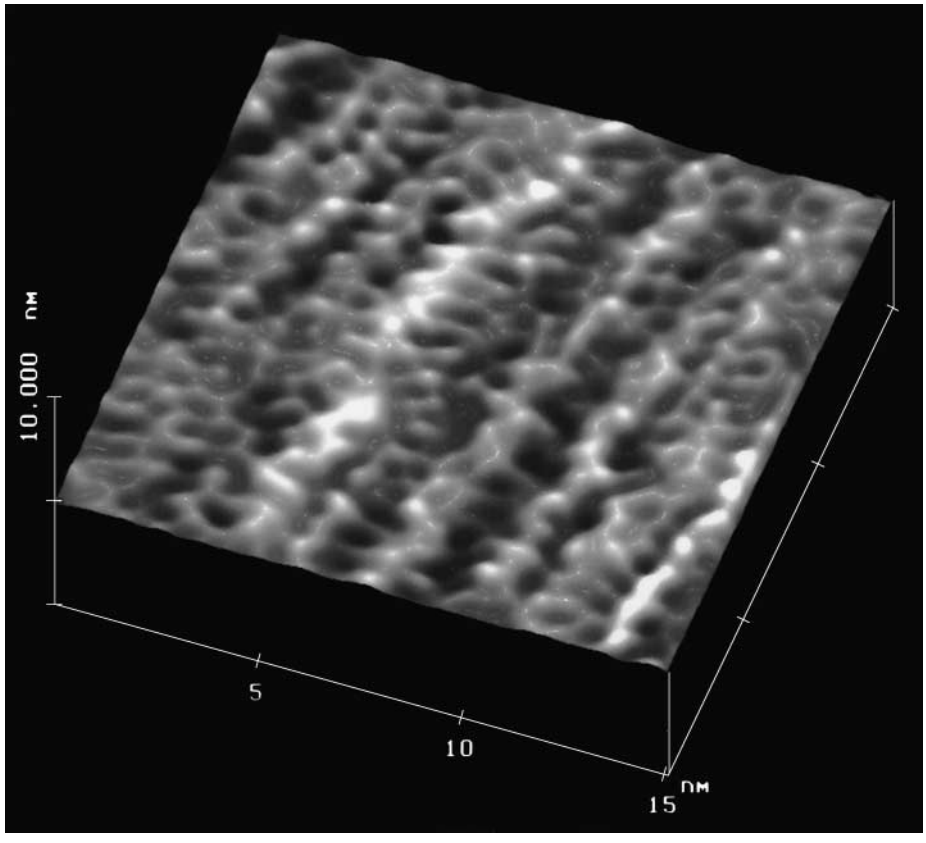

FIG. 3. Contact mode, nanometer-scale AFM image of the coked FCC surface after application of a 2D FFT routine with the FFT attenuation band cutoff set to 8.

centered at 2.2 ppm (with a shoulder near 4 ppm) assigned to silanol groups, while the broad line near 9.3 ppm is attributed to the presence of aromatic protons (17). In summary, NMR results in this case are of limited usefulness and can only indicate that the coke deposited in the FCC contains aliphatic chains as well as aromatic compounds.

The Density Functional Theory Method

The DFT formalism has in recent years received considerable attention as a way to describe the adsorption process at a gas/solid interface of pores with slitlike or cylindrical geometry (18). The ability of DFT to model physical adsorption provides a powerful method to extract surface area and pore size distribution results from experimental adsorption isotherms (18). The density functional approach to understanding the structure of inhomogeneous fluids at a solid interface consists of constructing the grand potential functional, $\Omega[\rho(r)]$, of the average singlet density $\rho(r)$ of the adsorptive at point r and minimizing $\Omega[\rho(r)]$ with respect to $\rho(r)$ to obtain the equilibrium density profile and thermodynamic properties,

$$\Omega[\rho(\mathbf{r})] = F[\rho(\mathbf{r})] + \int dr\,\rho(\mathbf{r})[V_{\text{ext}}(\mathbf{r}) - \mu_{\text{b}}], \qquad [1]$$

where μ_{b} is the bulk chemical potential of the adsorptive imposed on the system and $V_{\text{ext}}(r)$ is the wall potential at point r in 3D-space. At the equilibrium $\rho(r)$, the value of $\Omega[\rho(r)]$ will be a minimum. Thus by differentiating Eq. [1] with respect to the density $\rho(r)$ and equating this to zero, it is possible, at least in principle, to solve the resulting equation for the equilibrium density profile $\rho(r)$ at a free surface or in pores of a certain width by an iterative numerical method once expressions for $F[\rho(r)]$ and $V_{\text{ext}}(r)$ are known (19). The net quantity adsorbed at a given pressure is then found by integrating $\rho(r)$ from wall to wall and subtracting a quantity equivalent to the nonexcluded volume of the pore at the bulk gas density:

$$Q_{\text{ads}} = \int dz(\rho(z) - \rho_0(z)). \qquad [2]$$

The result is normalized to one square meter of wall area and expressed as cm^3 STP for direct comparison with experimental data.

For solids having a distribution of pore sizes, the integral equation of isothermal adsorption becomes

$$Q(p) = \int dH q(p,H) f(H), \qquad [3]$$

where $Q(p)$ is the total quantity of adsorbate per gram of adsorbent at pressure p; $q(p, H)$, the kernel function, describes the adsorption isotherm for an ideally homoporous material characterized by pore width H as quantity of adsorbate per square meter of pore surface, and $f(H)$ is the desired pore surface area distribution function with respect to H. The kernel functions derived from Eqs. [1] and [2] are used to fit Eq. [3] to experimental data using numerical methods. The generation of an adsorption isotherm will require the application of Eq. [3] over the entire pressure range considered; the limits of integration in Eq. [3] will be between the molecular diameter of the probe molecule and infinity (a free surface). Details of the procedure used to obtain SA and PV distribution data are given in Ref. 18; results are shown in the figures that follow.

Nitrogen Porosimetry Results

Heldemann and Botty (20) have reported that gas oil cracking over fresh and steam-aged silica-alumina catalysts generates a uniform distribution of coke and that the volume occupied by coke deposits coincide with the reduction of PV suffered by the catalysts; pore blocking and elimination of accessible surface area were not reported (20). Nitrogen adsorption and porosimetry results in Figs. 4–9 are consistent with these results. The isotherms in Fig. 4 are type I isotherms typical of microporous solids. After complete micropore filling, nitrogen uptake continues with increasing pressure owing to nitrogen adsorption in the FCC mesoporous structure. Near $p/P_o = 0.9$, there is a sharp increase in nitrogen uptake probably due to nitrogen condensation in the largest mesopores and macropores. It is clear from Fig. 4 alone that the coked catalyst has a reduced total pore volume, and the parallelism of the isotherms after micropore filling indicates little change in the mesopore structure. The small parallel loop hysteresis observed in Fig. 4 is typical of solids, such as FCCs, that contain slit-shaped mesopores resulting from the presence of kaolin platelets. Slit-shaped pores have been observed by AFM on the surface of several commercial FCCs (14–16) as well as in Figs. 1 and 2. The same data are plotted on a semilog scale in Fig. 5. It is seen that in the very low pressure region near $10^{-6} p/P_o$, nitrogen sorption is small in both catalysts. Below a relative pressure of 10^{-4}, the coked catalyst shows greater uptake of nitrogen, indicative of a stronger interaction perhaps caused by smaller micropores. The pore size distribution of these samples was determined by a method described in detail elsewhere (13, 18). The cumulative volume distribution in Fig. 6 suggests that coke deposition affects mainly pores with a diameter smaller than 1.0 nm. The plot in Fig. 7 more specifically indicates that coke deposition on the FCC micropore surface area causes the distribution of micropore sizes to shift to lower pore widths without significantly affecting pore sizes in the mesopore range.

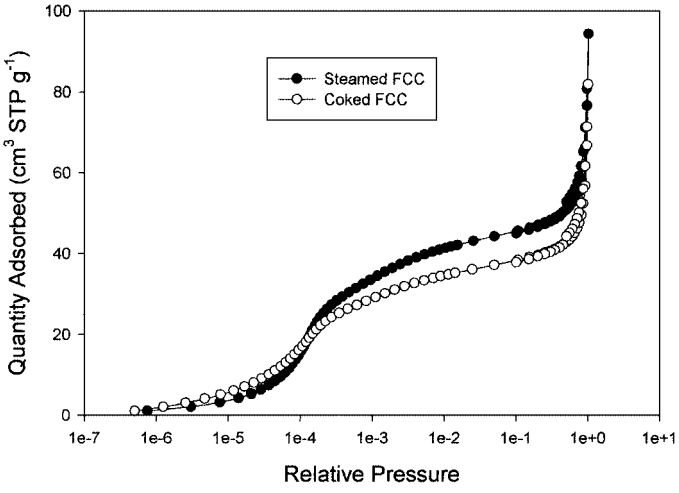

FIG. 5. Nitrogen sorption isotherms in the very low pressure range.

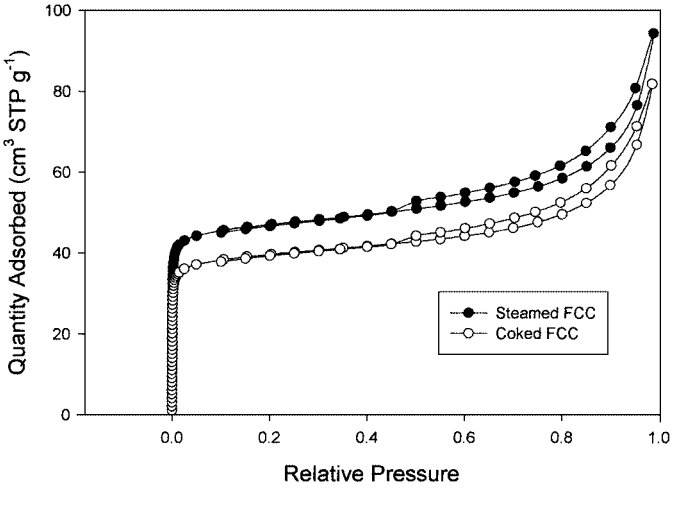

FIG. 4. Nitrogen sorption isotherms.

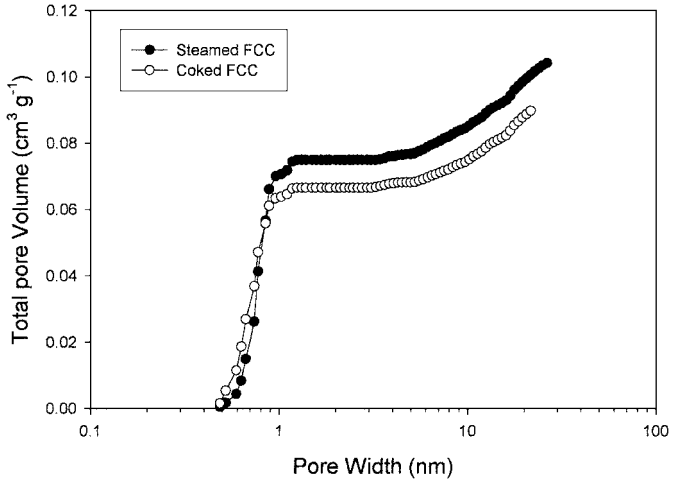

FIG. 6. Cumulative pore volume distribution as a function of the FCC pore width.

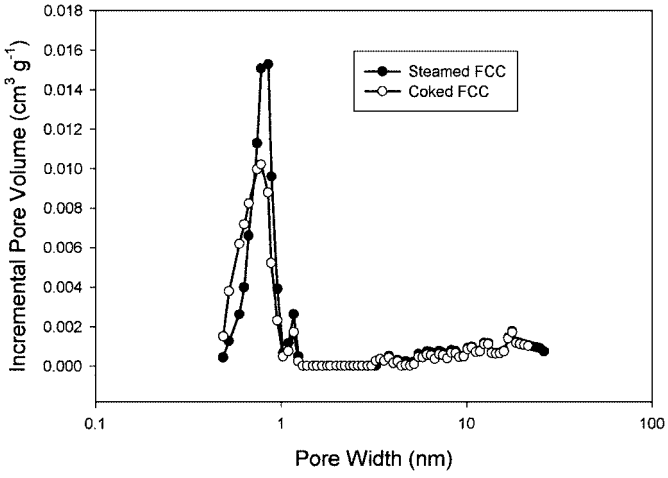

FIG. 7. Incremental pore volume obtained by fitting the hybrid DFT model to the adsorption isotherms.

Zeolite-free aluminosilicate FCCs of the type described by Heldemann and Botty (20) are mesoporous materials having an average pore diameter of 10 nm. In contrast, the pore size distribution data in Fig. 7 together with the sorption isotherms in Fig. 4 show that modern zeolitic FCCs are predominantly microporous solids. The reduction of pore volume resulting from the deposition of coke on the micropore walls is shown in Figs. 8–9. In Fig. 8 the change in the incremental pore volume between the coked and steam-aged FCC pore volume is plotted as a function of pore width. Coke deposition reduces pore width, and new pores with diameter in the 0.4–0.6 nm range and in the 0.85–1.0 nm range (not present in the steam-aged FCC) are formed. As a result, for pore width below ~0.6 nm and for pore width between 0.85 and 1.0 nm, the incremental pore volume difference increases (see Fig. 8). This difference starts to decrease when the pore widths of the micropores exceed 0.6 nm, it reaches zero near 0.7 nm, and then it becomes negative. After reaching a minimum near 0.85 nm it increases and remains essentially unchanged near zero for pore widths larger than 1.0 nm. In Fig. 9 differences in cumulative pore volume between the coked and steam-aged FCC are plotted. As seen before, coke deposition does not significantly affect the catalyst porosity in pores with width greater than about 1.0 nm. Above 4.0 nm there is a small increase in the pore volume difference owing to coke deposits in the FCC mesopores. Figure 9 can be interpreted to indicate that micropores between 0.6 and 1.0 nm suffer a loss of volume by narrowing, thus increasing relatively the micropore volume for pores with widths between 0.4 and 0.6 nm with a net loss in total pore volume. These results collectively indicate that, at MAT conditions, coke deposition in FCCs affects mainly the catalyst microspace while the mesoporosity present remains essentially unchanged by coke deposits and continues to provide access to the catalytically active microspace. Results similar to those in Figs. 7–9 (not shown) can be obtained by plotting area distribution as a function of pore width.

In Tables 2 and 3, results are compared to those of traditional methods. It can be seen that the BET and the Langmuir methods greatly underestimate the FCC surface area, a results that can be attributed to the fact that neither model allows for the filling of micropores. Surface areas derived from these two models will differ from the actual area in a way that depends on the solid microporous structure. Results in Tables 2 and 3 indicate that, for microporous solids such as FCCs, neither the BET nor the Langmuir methods can adequately represent the catalyst surface area. The *t*-plot method is designed to determine micropore volume, and the data in Tables 2 and 3 show PV values in reasonable agreement with those from DFT calculations. Like the *t*-plot method, the D–R technique

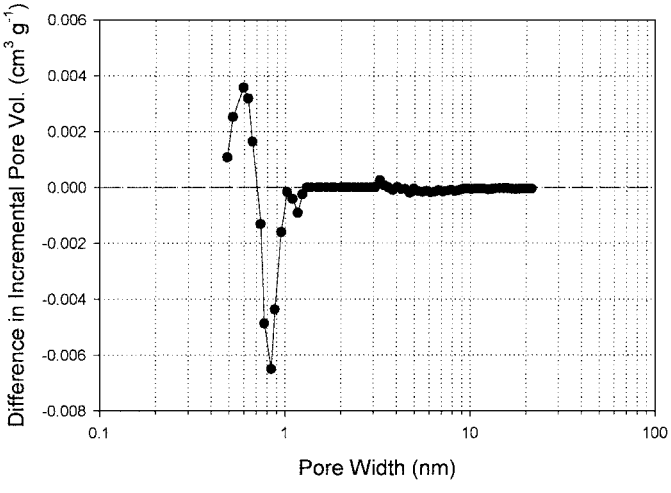

FIG. 8. Changes in the incremental pore volume difference between the coked and steam-aged FCC samples as a function of pore width.

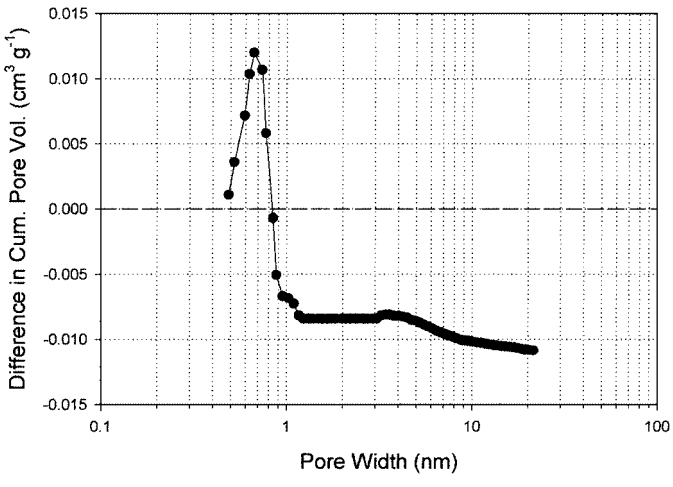

FIG. 9. Differences in cumulative pore volume between the coked and steam-aged FCC samples as a function of pore width.

(21) is meant to determine total micropore volumes. While empirical, the results for total pore volume are in good agreement with DFT data (Tables 2 and 3). However, the D–R and the *t*-plot methods give SA values that are unacceptably lower than those from DFT calculations; see Tables 2 and 3.

DFT results in Tables 2 and 3 show that after gas oil cracking, the FCC suffers a loss in total PV of 0.015 cm^3/g and that the loss of volume in the micropores is 0.009 cm^3/g. The skeletal density of extracted carbon from a catalyst used to crack gas oil has been determined to be 1.6 g/cm^3 (20). Thus the calculated volume occupied by 3.5% carbon is 0.022 cm^3/g, indicating that about 68% of the total carbon is located inside the FCC porous structure with the rest dispersed on the FCC surface. Moreover, 60% (0.009 cm^3/g) of the carbon deposited in the FCC porous structure is in micropores; the rest (0.006 cm^3/g) is in mesopores; see Tables 2 and 3.

As a concluding remark to the different SA and PV values reported in Tables 2 and 3, it should be noted the BET and Langmuir equations at best describe the adsorption isotherm of a nonmicroporous solid over a limited range of relative pressure. When appropriately applied, the monolayer adsorption capacity derived can be used to estimate a specific surface area that will be in reasonable agreement with results from more advanced methods such as density functional theory. For example, the BET surface area of a mesoporous silica-alumina support is 218 m^2/g, in reasonable agreement with a DFT value of 203 m^2/g.

On the other hand, when applied to microporous solids, the resulting adsorption capacity is not related in a simple way to specific surface area and the differences could be greatly magnified. For example, a zeolite with a faujasite structure gives a BET surface area of 606 m^2/g, much less than the value of 1236 m^2/g obtained by DFT. In this case, the small pore width, about 0.72 nm, does not permit a "monolayer" of nitrogen molecules to be formed.

Application of the BET or Langmuir method to isotherm data for microporous solids results in the attribution of the total micropore volume filling to free surface coverage. Whether this leads to over- or underestimation of the pore area depends on the pore dimensions. The area of pores less than about 3 molecular diameters in width will be greatly underestimated, while the area of micropores greater than about 1.4 nm will be significantly overestimated.

In the case of FCCs where both micro- and mesopores are present, the surface area determined from DFT will also depend on the geometry of the pore model used. The initial DFT models were developed for the study of activated carbons and were based on an assumed slit-pore geometry which generates a much smaller pore area for a given pore volume. This has led to the generation of FCC results in which surface areas were probably underestimated (16). In the current work, a cylindrical pore model is used that avoids this problem. In any case, the use of an advanced statistical mechanical model such as DFT is essential when studying materials, such as FCCs, having a broad spectrum of pore dimensions.

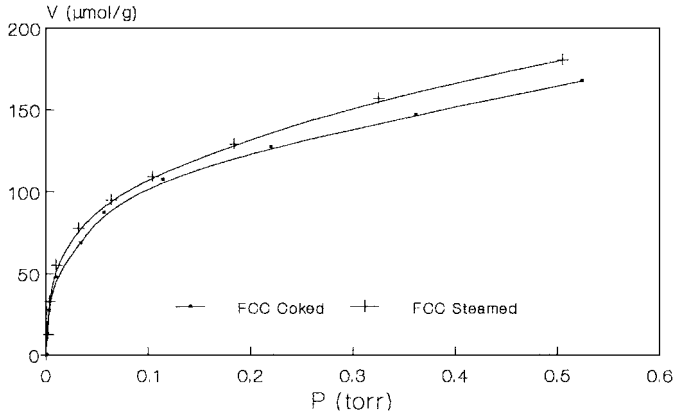

FIG. 10. Ammonia chemisorption isotherms of steam-aged and coked FCC samples.

Microcalorimetry Results

Ammonia chemisorption isotherms are shown in Fig. 10. The differences in NH_3 sorption shown in this figure reflect the loss of surface area and porosity that a steam-aged FCC experiences after coke deposition at MAT conditions. Not shown are secondary sorption isotherms, that is, sorption isotherms for samples after NH_3 adsorption and degassing in vacuum at 150°C. By subtracting the adsorbed volume of the secondary isotherms from that of the primary isotherms at the same equilibrium pressure ($p = 27$ Pa), it is possible to obtain V_{Irr}, the volume of irreversibly chemisorbed sorbate. This value is believed to correlate with the presence of strong (B + L) acid sites (11, 12). Although V_T, the total chemisorbed NH_3, decreases from 132 to 124 μmol NH_3/g in the coked FCC, V_{Irr} remains practically unchanged at 55 μmol NH_3/g; see Table 4. In this table, initial heats have been associated with the strength of the strongest acid sites present (11, 12). On the other hand, integral heats represent the total heat of adsorption evolved at $p = 27$ Pa and are therefore associated with the solid's acid site density.

The corresponding differential heats of ammonia adsorption as a function of coverage are shown in Fig. 11. As previously observed (16), steam aging generates a FCC with a porous structure containing a heterogeneous distribution of site strengths; the strength of these sites monotonically decreases with NH_3 coverage (Fig. 11). The effect of coking is to decrease acid site density and strength. In fact, integral heats (the total heat of adsorption evolved at $p = 27$ Pa) decrease to 6.4 from 7.4 J/g while initial heats (the strength of the strongest acid sites) decreases to 144 from 156 kJ/mol (Fig. 11). The data in Table 4 indicate that coking reduces both the strength of the strongest acid sites as well as the

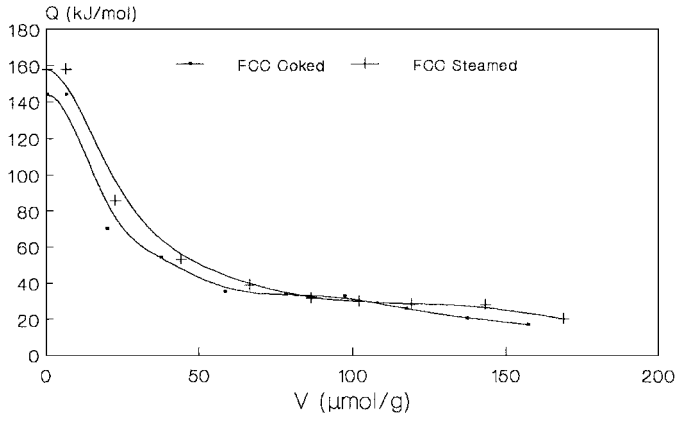

FIG. 11. Differential heat profiles of steam-aged and coked FCC samples.

number of acid sites present. Acidity losses indicated in Table 4 are minor compared to those experienced by fresh FCCs during steam aging (16).

SUMMARY AND CONCLUSIONS

The structure, composition, and distribution of coke deposits in heterogeneous catalysts during hydrocarbon conversion reactions is and will probably remain a subject of controversy and debate (1). During gas oil conversion with FCCs, the structure and location (and composition) of coke deposits will depend on feedstock and catalyst properties as well as on reactor conditions. At the MAT conditions (cracking and stripping) used in this study to evaluate FCCs in the laboratory, catalyst deactivation occurs because of interactions between the FCC active sites and carbon deposits; evidence of preferential coke deposition near the FCC pore's mouth and suppression of active surface area from the cracking process was not observed at the stripping conditions used.

During gas oil cracking at MAT conditions, coke is deposited inside as well as outside a pillared rectorite catalyst microspace yielding AFM images (5) that are geometrically similar to calculated images for graphite (5, 22). In contrast, the same cracking reaction form carbonaceous deposits on a commercial FCC surface that are imaged as raised surface features consisting of chains of atoms and molecules (Fig. 3).

Nitrogen porosimetry results show that only 32% of the total coke (carbon) generated is located on the FCC surface. The rest is distributed in a 60%/40% ratio between the FCC micropores and mesopore. Coke uniformly coats the micropore walls, thus decreasing their pore size. As a result there are moderate declines in acid site strength and density. Both the BET and Langmuir equations grossly underestimate the FCC total surface area and the use of the DFT method is strongly recommended to study the porosity of FCC samples.

ACKNOWLEDGMENTS

This work has been supported in part by NATO collaborative Grant CRG-971497 to M.L.O. Special thanks are due to Mr. J. Gonzales (Akzo Nobel) for MAT data, to Prof. S. Gould for AFM images, and to Dr. M. Kalwei for NMR data.

REFERENCES

1. Wolf, E. H., and Alfani, A., *Catal. Rev. Sci. Eng.* **24**, 329 (1982).
2. McIntyre, B. J., Salmeron, M., and Samorjai, G. A., *J. Catal.* **164**, 184 (1999).
3. Trimm, D. L., *in* "Progress in Catalysts Deactivation" (J. L. Figueiredo, Ed.), p. 65. Nijhoff, The Hague/Boston/London, 1982.
4. Gaigneauex, E. M., Ruiz, P., Wolf, E. E., and Delmond, B., *J. Catal.* **172**, 247 (1997).
5. Occelli, M. L., and Gould, S. A. C., *J. Catal.* **198**, 41 (2001).
6. Hall, P. J., Snape, C. E., Brown, S. D., Diaz, M. C., Hughes, R., Koon, C. L. A., and Calo, J. M., *Ind. Eng. Chem. Res.* (in press).
7. Barret, E. P., Joyner, L. S., and Halenda, P. P., *J. Am. Chem. Soc.* **73**, 373 (1951).
8. Langmuir, I., *J. Am. Chem. Soc.* **38**, 2267 (1916).
9. Brunauer, S., Emmett, P. H., and Teller, E., *J. Am. Chem. Soc.* **60**, 309 (1938).
10. Olivier, J. P., and Occelli, M. L., *J. Phys. Chem.* **105**, 623 (2001).
11. Auroux, A., *in* "Catalyst Characterization: Physical Techniques for Solid Materials" (B. Imelik and J. C. Vedrine, Eds.), Chap. 22. Plenum Press, New York, 1994.
12. Auroux, A., *Top. Catal.* **4**, 71 (1997).
13. Olivier, J. P., and Conklin, W. B., presented at "First International Symposium on Effects of Surface Heterogeneity in Adsorption and Catalysis on Solids," Kazimierz Dolny, Poland, 1992.
14. Occelli, M. L., Gould, S., and Drake, B., *in* "Fluid Catalytic Cracking III: Materials and Processes" (M. L. Occelli and P. O'Connor, Eds.) ACS Symp. Ser. Vol. 571, p. 20. American Chemical Society, Washington, DC, 1994.
15. Occelli, M. L., Gould, S. A. C., Baldiraghi, F., and Leoncini, S., *in* "Fluid Cracking Catalysts" (M. L. Occelli and P. O'Connor, Eds.), p. 227. Marcel-Dekker, New York, 1998.
16. Occelli, M. L., Eckert, H., Wolker, A., Kalwei, M., Auroux, A., and Gould, S. A. C., *J. Catal.* **196**, 134 (2000).
17. Kalwei, M., private communication, 2000.
18. Olivier, J. P., Koch, S., Jaroniec, M., and Kruk, M., *in* "Characterization of Porous Solids V" (K. K. Unger *et al.*, Eds.), Studies in Surface Science, Vol. 128, p. 71. Elsevier Amsterdam, 2000.
19. Olivier, J. P., *in* "Surfaces of Nanoparticles and Porous Materials" (J. A. Schwarz and C. I. Contescu, Eds.), p. 295. Marcel-Dekker, New York, 1999.
20. Haldemann, R. G., and Botty, M. C., *J. Phys. Chem.* **63**, 489 (1959).
21. Dubinin, M. M., and Radushkevich, L. V., *Dokl. Akad. Nauk. SSSR* **55**, 331 (1947).
22. Gould, S. A. C., Burke, K., and Hansma, P. K., *Phys. Rev. B* **40**, 5363 (1989).